Skip to main content

You're seeing our new journal sites and we'd like your opinion, please send feedback

Arabian Journal of Geosciences

The official journal of the **Saudi Society for Geosciences**, the Arabian Journal of Geosciences examines the entire range of earth science topics focused on, but not limited, to those that have regional significance to the Middle East and the Euro-Mediterranean Zone.

The journal features peer-reviewed original and review articles on such topics as: geology, hydrogeology, earth system science, petroleum sciences, geophysics, seismology and crustal structures, tectonics, sedimentology, palaeontology, metamorphic and igneous petrology, natural hazards, environmental sciences and sustainable development, geoarchaeology, geomorphology, paleo-environment studies, oceanography, atmospheric sciences, GIS and remote sensing, geodesy, mineralogy, volcanology, geochemistry and metallogenesis. — show all

- The official journal of the Saudi Society for Geosciences
- Examines the entire range of earth science topics
- Coverage focused on, but not limited to, issues that have regional significance to the Middle East and North Africa

Skip to main content

Arabian Journal of Geosciences
All Volumes & Issues
ISSN: 1866-7511 (Print) 1866-7538 (Online)

In this issue (16 articles)

Geochemical characteristics and significances of C_{19}-C_{26} short-chain steranes in crude oils from the Western Qaidam Basin, China

Min Zhang, *Wenyu Zhang*, *Qingsong Cheng*, *Qing Yuan* Article:106

11. Original Paper

Estimation of behavioral change of SSC of bed profile in the river using ADCP

Atul Kumar Rahul, *Nikita Shivhare*, *Shyam Bihari Dwivedi*... Article:105

12. Original Paper

Study on fracture process zone near mode II and mode III dynamic crack tip

Chenmeng Ji, *Chengzhi Qi*, *Liren Ban* Article:104

13. Original Paper

Experimental study on contact angle and pore characteristics of compacted loess

Yanlin Jing, *Zhiquan Zhang*, *Wei Tian*, *Xin Wen*... Article:103

14. ICWEES2018 & IWFC2018

Topical Collection

Trend analysis of river flow and groundwater level for Shipra river basin in India

Ravi Venkatrao Galkate, *Shalini Yadav*... Article:102

15. Original Paper

Assessment of groundwater quality in Southern Saudi Arabia: case study of Najran area

Hussain Jaber Alfaifi, *Ali Yahya Kahal*, *Kamal Abdelrahman*... Article:101

16. Original Paper

Robust interpretation of single and multiple self-potential anomalies via flower pollination algorithm

Sungkono Article:100

Support

Editors

FOUNDER *of* AJGS
Abdullah Al-Amri: King Saud University, Riyadh, Saudi Arabia

EDITOR-IN-CHIEF
Abdullah Al-Amri: King Saud University, Riyadh, Saudi Arabia
Email: alamri.geo@gmail.com

TOPICAL CHIEF EDITORS

T 1. **Zhihua Zhang:** Shandong University, Jinan, China
T 2. **Haroun Chenchouni:** University of Tebessa, Algeria
T 3. **Jianxiong Chen:** Anadarko Petroleum, Houston, TX, USA
T 4. **Amjad Kallel:** ENIS, University of Sfax, Tunisia
T 5. **Narasimman Sundararajan:** Sultan Qaboos University, Muscat, Oman
T 6. **Biswajeet Pradhan:** University of Technology Sydney, Sydney, Australia
T 7. **Domenico Doronzo:** Spanish National Research Council, Spain
T 8. **Zeynal Abiddin Erguler:** Dumlupinar University, Kutahya, Turkey
T 9. **Stefan Grab:** School of Geography, University of the Witwatersrand, South Africa
T 10. **Broder J. Merkel:** TU Bergakademie Freiberg, Freiberg, Germany
T 11. **Marina Rabineau:** IUEM, Université de Brest, France
T 12. **Murat Karakus:** University of Adelaide, Australia
T 13. **Santanu Banerjee:** Indian Institute of Technology Bombay, Mumbai, India
T 14. **Beatriz Bádenas:** University of Zaragoza, Zaragoza, Spain
T 15. **François Roure:** IFP – Energies Nouvelles, France

COVERED TOPICS, TOPICAL CHIEF EDITORS *and* ASSOCIATE EDITORS

Topic 1. Atmospheric Sciences, Meteorology, Climatology, Oceanography
Chief Editor: Zhihua Zhang, China

Ali Al-Dousari: Kuwait Institute for Scientific Research, Safat, Kuwait
Daniele Contini: Institute of Atmospheric Sciences and Climate, NRC Italy, Lecce, Italy
Muhammad Jawed Iqbal: University of Karachi, Karachi, Pakistan
Abdelkader Mezghani: Norwegian Meteorological Institute, Norway
Zhien Zhang: The Ohio State University, US
Huakun Zhou: Chinese Academy of Sciences, Xining, China

Topic 2. Biogeochemistry, Geobiology, Geoecology, Geoagronomy
Chief Editor: Haroun Chenchouni, Algeria

Md. Saiful Islam: Patuakhali Science and Technology University(PSTU), Patuakhali, Bangladesh

Topic 3. Earthquake Seismology and Geodesy
Chief Editor: Jianxiong Chen, USA

Mohamed Amrouche: Schlumberger, Tokyo, Japan
Ali Dehghani: University of Hamburg, Hamburg, Germany
Longjun Dong: Central South University, Changsha, China
Mehdi Eshagh: University West, Trollhättan, Sweden
Jianping Huang: China University of Petroleum, Dongying, China
Lun Li: Sun Yat-sen University, Guangzhou, China
Mustapha Meghraoui: University of Strasbourg, Strasbourg, France

Topic 4. Environmental Earth Sciences
Chief Editor: Amjad Kallel, Tunisia

Paromita Chakraborty: SRM Inst. of Science and Technology, Chennai, India
Sudip Chakraborty: University of Calabria, Rende, Italy

Topic 5. Exploration & Theoretical Geophysics, Seismic & Well Logging Methods, Mathematical Geosciences
Chief Editor: Narasimman Sundararajan, Oman

Topic 6. Geo-Informatics and Remote Sensing
Chief Editor: Biswajeet Pradhan, Australia

Topic 7. Geochemistry, Mineralogy, Petrology, Volcanology
Chief Editor: Domenico Doronzo, Spain

Topic 8. Geological Engineering, Geotechnical Engineering

Chief Editor: Zeynal Abiddin Erguler, Turkey

Zhen-Dong Cui: China University of Mining and Technology, Xuzhou, Jiangsu, China
Dave Giles: University of Portsmouth, UK
Sanjay Kumar Shukla: School of Engineering, Edith Cowan University, Perth, Australia
Giacomo Pepe: Università di Genova, Genova, Italy
Ahmed Salih Mohammed: University of Sulaimani, Kurdistan region, Iraq
Kejun Wen: Jackson State University, USA

Topic 9. Geomorphology, Geography, Soil Science, Glaciology, Geoarchaeology, Geoheritage
Chief Editor: Stefan Grab, South Africa

Davide Baioni: Università degli Studi "CarloBo" di Urbino, Italy
Sheryl Luzzadder-Beach: The University of Texas at Austin, TX, USA
Lisa Mol: University of West England, Bristol, UK
Kosmas Pavlopoulos: Paris Sorbonne University Abu Dhabi, UAE
Adriano Ribolini: Dipartimento di Scienze della Terra,Università di Pisa, Italy

Topic 10. Hydrology, Hydrogeology, Hydrochemistry
Chief Editor: Broder J. Merkel, Germany

Maurizio Barbieri: University of Rome La Sapienza, Italy
Helder I. Chaminé: School of Engineering - ISEP, Polytechnic of Porto, Portugal
Mingjie Chen: Sultan Qaboos University, Muscat, Oman
Lassâad Dassi: University of Sfax, Sfax, Tunisia
Tajudeen Muhammad Iwalewa: Harvard University, Massachusetts, USA
Ozgur Kisi: Ilia State University, Tbilisi, Georgia
Elango Lakshmanan: Dept. of Geology, Anna University, Chennai(Madras), India
Pradeep Naik: Rajiv Gandhi National Ground Water Training & Research Institute, India
Fernando A.L. Pacheco: Trás-os-Montes and Alto Douro University – UTAD, Portugal
Angela Vallejos: Polytechnic School, University of Almeria, Spain
Haw Yen: Blackland Research & Extension Center, Texas A&M University, USA
Lahcen Zouhri: Institut Polytechnique La Salle Beauvais, France

Topic 11. Marine Geosciences, Historical Geology, Paleoceanography, Paleoclimatology
Chief Editor: Marina Rabineau, France

Daniel Aslanian: IFREMER, Lab. LGS, Plouzané, France
Franck Bassinot: LSCE (CEA-CNRS-UVSQ), Gif-sur-Yvette, France
Gurumurthy Gundiga: Birbal Sahni Institute of Palaeosciences, India
Nadia Mhammdi: Institut Scientifique, Université Mohammed V, Rabat, Morocco
Dominico Ridente: University of Roma, Italy

Topic 12. Numerical and Analytical Methods in Mining Sciences and Geomechanics
Chief Editor: Murat Karakus, Australia

Khalid Amrouch: The University of Adelaide, Australia
Feng Dai: Sichuan University, Chengdu, Sichuan, China
Sebnem Duzgun: Colorado School of Mines, USA
Wissem Frikha: National School of Engineers of Tunis, Tunisia

Topic 13. Petroleum and Energy Engineering, Petroleum Geochemistry
Chief Editor: Santanu Banerjee, India

Topic 14. Sedimentology, Stratigraphy, Paleontology, Geochronology
Chief Editor: Beatriz Bádenas, Spain

Topic 15. Structural Geology, Tectonics and Geodynamics, Petroleum Geology
Chief Editor: François Roure, France

Arabian Journal of Geosciences (2020) 13:100
https://doi.org/10.1007/s12517-020-5079-4

ORIGINAL PAPER

Robust interpretation of single and multiple self-potential anomalies via flower pollination algorithm

Sungkono[1]

Received: 10 August 2018 / Accepted: 7 January 2020

Abstract

Self-potential (SP) method is suitable for identifying positions of fractures, ore bodies, leakage, corrosion of metal, etc. The identification of SP anomalies can be implemented through inversion process, which not only serves to determine the best model parameters but also to estimate their uncertainties. The model parameters and their uncertainty can be determined from the posterior distribution model (PDM) of the SP anomaly inversion. To find the required PDM, in this paper, generalized likelihood uncertainty estimation (GLUE) thresholding is proposed as a joint approach together with flower pollination algorithm (FPA). This overall method is then tested on several synthetics and fields (i.e., metallic drum, Weiss, Sawoo, and LUSI anomalies) SP data containing single and multiples of SP sources. The results demonstrate that the proposed algorithm is robust for solving quantitative interpretations of SP data. Moreover, this method does not require prior assumptions over the shape of the anomaly source.

Keywords Uncertainty model parameters · SP parameters · robust algorithm · GLUE threshold

Introduction

SP method is a passive method of measuring natural potentials resulting from three different sources including thermoelectric, electrochemical, and electrokinetic sources. SP data is commonly used in mining, geotechnical, and environmental studies (Al-Saigh et al., 1994; Biswas, 2017; Bolève et al., 2012; Lapenna et al., 2003; Maineult et al., 2013; Mehanee, 2014; Rozycki et al., 2006; Yüngül, 1950). Analysis SP data can be divided into two groups including inversion and signal processing (Hilbert transform, fast Fourier transform, and continuous wavelet transform) (Biswas and Sharma, 2014a; Di Maio et al., 2016a, 2016b; Jagannadha Rao et al., 1993; Mauri et al., 2010, 2011; Patella, 1997; Soueid Ahmed et al., 2013).

However, because the solution produced in inversion process is generally not unique, the geophysical inversion, especially in SP data inversion, not only serves to determine the model parameters correlating to the best objective function but also to provide posterior distribution model (PDM) (Biswas and Sharma, 2014a, 2015, 2017; Li and Yin, 2012; Pekşen et al., 2011; Sharma and Biswas, 2013). The model parameter uncertainty produced via inversion process depends on robustness optimization method based upon estimation, likelihood, and noise containing in the data (Sadegh et al., 2015; Scharnagl et al., 2011; Vrugt and Beven, 2018). To eliminate likelihood and effects of noise properties in the PDM, Beven and colleagues (Beven, 2006; Beven and Binley, 2014; Beven and Smith, 2015) have proposed a method called generalized likelihood uncertainty estimation (GLUE).

GLUE is one possible strategy to generate posterior distribution model (PDM) without requiring former knowledge of noise properties contained within the data. In most cases, to deliver PDM, GLUE should be combined with Markov chain Monte Carlo (MCMC) (Blasone et al., 2008; Li et al., 2010; Vrugt, 2016) or the other global optimum methods (Cho and Olivera, 2014).

Cho and Olivera (2014) demonstrated that particle swarm optimization (PSO) combined with GLUE has proven fast and accurate in producing PDM. However, some literatures show that flower pollination algorithm (FPA) outperformed PSO and genetic algorithm for several applications (Yang, 2012). Additionally, FPA also has great advantages in simplicity and flexibility. This method is still rarely used in geophysical data

Responsible Editor: Dikun Yang

✉ Sungkono
hening_1@physics.its.ac.id

[1] Department of Physics, Institut Teknologi Sepuluh Nopember, Surabaya, Indonesia

Published online: 21 January 2020

inversion. Therefore, in this paper, FPA is proposed as a faster and more robust approach towards delivering PDM in self-potential data inversion. To verify the proposed approach, the algorithm is tested onto several synthetics and fields of SP data.

Self-potential method

General and field procedure

Sources of SP method have been clearly described by Revil and Jardani (2013) which include (1) thermo potential and natural potential related to temperature different; (2) electrochemical, as a source of different potential caused by chemical reaction; (3) streaming potential or electrokinetic, which is related to ground water flow; and (4) geobattery, which explains about potential difference caused by biotic and abiotic (corrosion of ore body, organic-rich contaminant plumes) to redox reaction. In addition, electrochemicals are combined by both diffusion and Nernst potentials. Diffusion potential is affected by different ionic concentrations between the pore water of the formation and the environment, while Nernst potential is variation in electrolyte concentration caused by different electrochemical reactions at each electrode (two identical electrodes).

Furthermore, Revil and Jardani (2013) also describe the measurement and correction of SP data. Self-potential data is the potential different measured using non-polarizing electrodes connected to high sensitivity and high input impedance measurement device. To measure potential difference, two measurement types can be used including fix based and gradient approaches. In the fix-based measurement, one electrode is fixed as the based station while other electrodes move, where gradient potential is measured with both electrodes in motion.

After SP data is acquired, the data must be corrected using two steps, which can include reference and closure corrections. Reference correction must be applied when the position of the reference (fix based) electrode has changed, while closure correction is used for drift correction and to reduce the effect of the measurement conditions (e.g., soil moisture, soil temperature, instrument error, etc.).

Forward modeling

Forward modeling method describes that theoretical responses (data) are calculated using assumed model parameters and depends on two sets of variables. In forward modeling, data on the SP response, the set of available locations of the observation points, and the set of model parameters (variables reflecting the physical properties and geometry of the subsurface structure) must be known. Forward modeling is needed during interpretation of field data, where the interpretation can be done using manual matching through repeated forward modeling or using automatic inversion.

In general, SP response depends on the location of positive and negative poles, electric dipole density, and the shapes of anomalies. Most field studies are generally described as standard geometrical shapes, including horizontal cylinder, vertical cylinder, and spherical bodies. Figure 1a shows a cross section of sphere and horizontal cylinder models, while Fig. 1b demonstrates a cross section of semi-infinite vertical cylinder model. The SP response $v(x_i)$ for vertical cylinder, horizontal cylinder, and sphere models in subsurface which is measured in the surface x_i can be described as follows

$$v(x_i) = K\frac{(x_i - D)\cos(\theta) + h\sin(\theta)}{\left((x_i - D)^2 + h^2\right)^q} \quad (1)$$

where D denotes the position of the center anomaly from the start of measurement point while h describes the depth of the center source body. K and θ describe the polarization magnitude and angle, respectively. Moreover, q is shape factor which can be valuable 0.5, 1.0, and 1.5 for semi-infinite vertical cylinder, horizontal cylinder, and sphere, respectively. SP response for multiple anomalies is calculated by summing up the potential generated by individual targets as the SP response (Biswas and Sharma, 2014b).

Flower pollination algorithm

The flower pollination algorithm (FPA) was developed by Yang (2012) which was inspired by the pollination process for flowering plants. Pollination is the process of pollen grain transfer from the male part of the flower to the ovule in the female part via abiotic (e.g., water and wind) and biotic (e.g., bees, bats, butterflies, and birds) pollinators.

Pollination can be acquired through self-pollination and cross-pollination (Fig. 2). Self-pollination describes the transfer of pollen from the male to female parts within one flower plant or to another flower of the same plant species. Self-pollination generally needs no pollinators. In cross-pollination, pollens are transferred from one flower to another of a different plant. Wherefore, cross-pollinations occur in long distances and being generally resulted by bees, birds, and bats.

Based on this description of the pollination process and behavior of pollinators, four rules can be stated:

1. Cross-pollination and biotic are deliberated processes for global pollination, where pollinators move using Lévy flights.
2. Self-pollination and abiotic pollination represent local pollination.

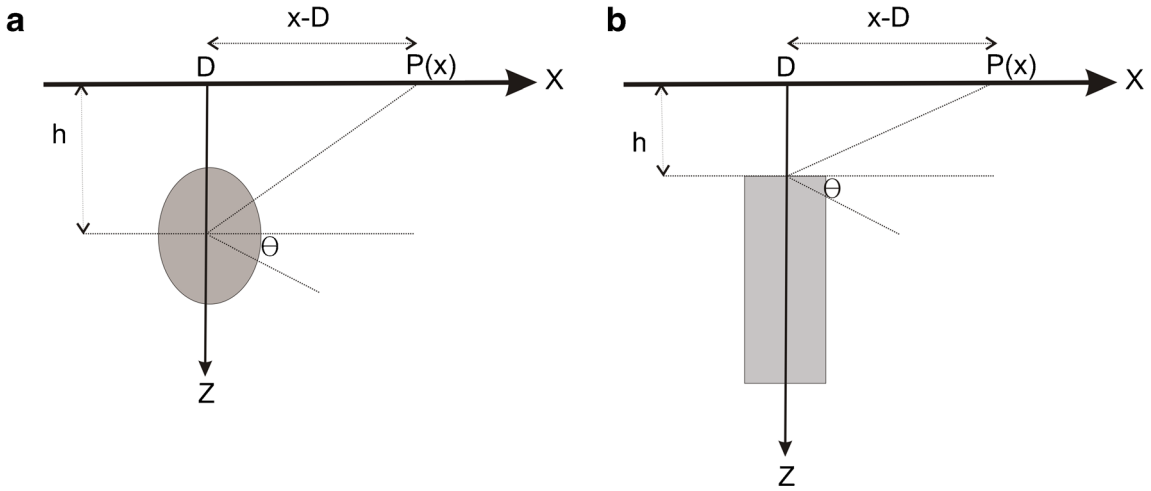

Fig. 1 Geometry shape bodies. (a) Sphere and horizontal cylinder models, (b) semi-infinite vertical cylinder model (b)

3. Pollinators are able to develop flower constancy, which is equivalent to the probability of a reproduction, correlative to the similarity of two flowers involved.
4. The interaction of global and local pollinations is controlled by probability $p \in [0, 1]$.

Concept of FPA

In order to be applied for optimization or inversion, four rules must be converted into proper equations. The rules 1 and 3 describe that in the global pollination step, flower pollen gametes are carried by pollinators (viz., insects, birds, bats, and other animals) and, as a result, may travel over long distances because insects can often fly and move in a much longer range. Consequently, both rules can be represented mathematically as:

$$s_i^{t+1} = s_i^t + \alpha L(\lambda)\left(s_i^t - gbest\right) \tag{2}$$

where s_i^t describes the pollen i or solution vector s_i at iteration t and $gbest$ denotes the current best solution found among all solutions at the current iteration. Here, αdescribes a scaling factor to control the step size, while $L(\lambda)$ is a step size parameter. The $L(\lambda)$ reflects the strength of the pollination. Because insects travel over a long distance with various distance steps, the step size in FPA $L(\lambda)$ uses Lévy distribution.

Additionally, the local pollination (both Rule 2 and Rule 3) can be written as follows:

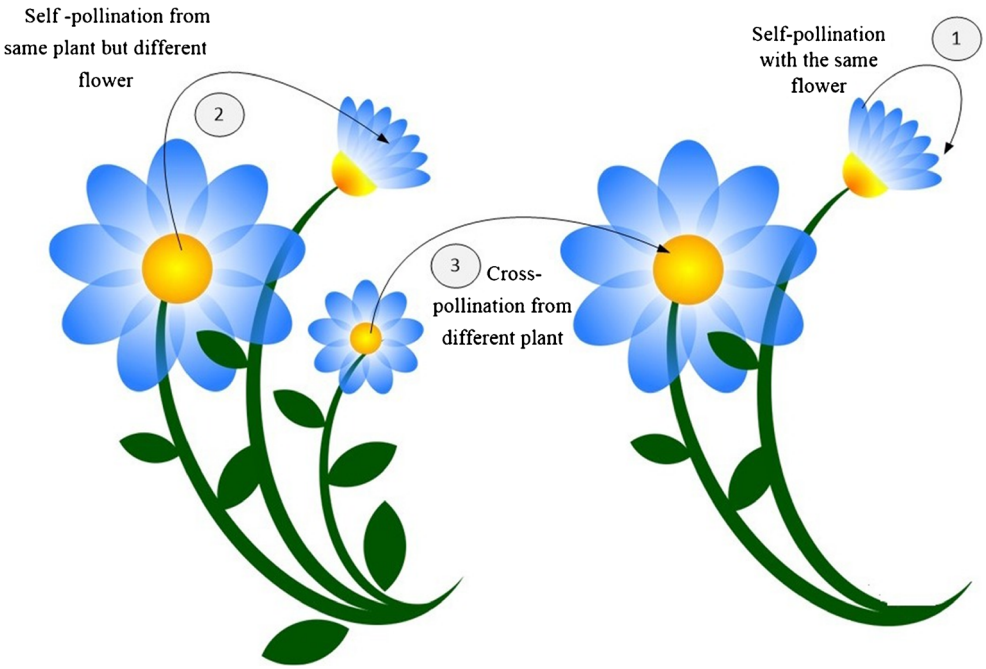

Fig. 2 Flower pollination methods; (1) and (2) denote self-pollination, and (2) cross-pollination from different plant (Nasser et al., 2018)

$$s_i^{t+1} = s_i^t + \in\left(s_l^t - s_j^t\right) \tag{3}$$

where s_k^t, s_l^t, and s_j^t describe the pollen obtained from each different flower of the same plant species. It means that the index $i \neq l \neq j$. Here, $\in$ denotes a uniform distribution in [0, 1]. Mathematically, the equation is equivalent to a local random walk and a crossover equation in the differential evolution.

As other global algorithms, FPA also uses several populations, called pollen, to create solution. The overall FPA engages iterative steps which can be summarized as in Appendix A. Firstly, FPA is initiated by generating a random number of pollen population as candidate solutions. Secondly, the objective function for each population is estimated. Thirdly, a number of population of random value in [0, 1] is generated. When the random value is lower than the interaction probability p, the pollen s_i^{t+1} is calculated using Eq. (2) otherwise the pollen s_i^{t+1} is estimated through Eq. (3). After determining new pollens, all of the pollens are evaluated using greedy selection to determine pollens that can survive for the next generation. The selection operator is described below:

$$s_i^{t+1} = \begin{cases} s_i^{t+1} & if \quad f\left(s_i^{t+1}\right) \leq f\left(s_i^t\right) \\ s_i^t & if \quad f\left(s_i^{t+1}\right) > f\left(s_i^t\right) \end{cases} \tag{4}$$

In the current population, a new pollen is updated when the objective function value of the new pollen is equal or less than that the previous pollen. The new pollen is then selected as the population of pollen for further iteration; otherwise, the previous pollen remains as the population of pollen for further iteration. The process then goes back in the third step. The FPA process will continue until the stopping criterion is met. Detailed step of the FPA is explained in Appendix A.

FPA properties

In inversion process, two certain behaviors present in an algorithm are exploration and exploitation. Exploration property is suited towards providing PDM parameters, while exploitation is to find convergences quickly. In order to inverse SP data, balancing the two properties are required. In fact, every global optimization analysis depends on balancing exploration and exploitation behaviors. Both properties are defined implicitly and are affected by FPA parameters (Łukasik and Kowalski, 2015; Yang, 2012).

FPA also contains two properties which are long-distance pollinators (Eq. 2) and flower consistency (Eq. 3). The first property describes that pollinators (i.e., insects) are able to travel long distances. Consequently, they can avoid trap of any local optimum and can explore the larger search space of model parameters. In the manner, the first property reflects exploration moves. Meanwhile, flower consistency ensures that the same species of the flowers are chosen more frequently and thus guarantee quicker convergence. This step is essentially an exploitative move.

In principle, flower pollination activities can occur at both global and local optimizations, depending on the interaction probability p. The parameter can be effectively used to switch between global pollination and intensive local pollination. Additionally, FPA also depends on a scaling factor. A preliminary parametric study indicates that $p = 0.8$ and $\alpha = 0.1$ worked for most applications (Yang, 2016).

Inversion of SP data using FPA

Inversion process is done to automatically determine model parameters m, generally by using an algorithm including local and global optimizations. Some algorithms for inverting process need an objective function to fit between observed $V^o = \left[V_1^o, V_2^o, \cdots, V_N^o\right]$ and calculated $V^c = \left[V_1^c, V_2^c, \cdots, V_N^c\right]$ SP response. It means that the objective function generally contains L-2 norm of observed and calculated SP response for minimizing. The objective function $f(m)$ is used to invert process in this manuscript which is described as follows (Monteiro Santos, 2010)

$$f(m) = \frac{2\left\|V_i^o - V_i^c(m)\right\|}{\left\|V_i^o - V_i^c(m)\right\| + \left\|V_i^o + V_i^c(m)\right\|} \quad i = 1, 2, \cdots, N \tag{5}$$

where N indicates the number of measured data. Furthermore, the misfit between measured and calculated SP data is calculated using the average relative error (in %) as:

$$misfit(\%) = \frac{100}{N}\sqrt{\sum_{i=1}^{N}\left(\frac{V_i^o - V_i^c(m)}{V_i^o}\right)^2} \tag{6}$$

Equation (4) shows that the calculated SP data and objective function depend on the model parameter. Model parameters m contains D, h, K, θ, and q which can be transcribed as $m = [K_1, \cdots, K_M, D_1, \cdots, D_M, h_1, \cdots, h_M, \theta_1, \cdots, \theta_M, q_1, \cdots, q_M]$ with M as the number of anomalies. Inversion process using FPA is done through solution vectorss_i in the Eq. (2) and (3) equal to model parameters. Additionally, SP data inversion using FPA is to minimize objective function (Eq. 5).

PDM via GLUE threshold

In order to PDM, a GLUE threshold of the best fit is set as an input for this approach. The threshold value can be determined before or after inversion processing. The GLUE thresholding used is similar to one described by Fernández-Martínez et al. (2012). The threshold value of the objective function should reflect the observational noises, together with the impact of error in physical assumptions (e.g., homogeneity, isotropy, and anisotropy) in forward modeling

and/or impact of errors of numerical approximations within the forward mathematical model (Beven and Binley, 2014; Biswas and Sharma, 2014a; Jackson, 1972; Sharma and Biswas, 2013; Sungkono and Santosa, 2015).

In the inversion process, all pollens s_i^{t+1} may become the posterior candidate when the pollens for each iteration fulfills the criterion $f(s_i^{t+1}) \leq f(s_i^t)$. After the FPA iteration concludes, PDM is selected from the posterior candidate using GLUE threshold. Model parameter uncertainty is then delivered when the objective function is less than the objective function threshold (*tol*) which can be described as follows (Fernández-Martínez et al., 2012):

$$f(m) \leq tol \tag{7}$$

Using Eq. (7), all model parameters with an objective function or misfit below the threshold or tolerated value are included into the PDM. In this way, the GLUE threshold is simpler and more flexible for case of global optimization because the threshold value can be applied after the inversion process (Laby et al., 2016). *Consequently, the PDM and their statistics depend on the threshold value. After PDM is provided using global optimization and GLUE threshold, best model parameters and their uncertainty can be estimated through median or average and standard deviation or interquartile as in the various literatures* (Biswas and Sharma, 2017, 2015, 2014b, 2014a; Ramadhani and Sungkono, 2019; Sungkono and Santosa, 2015; Sungkono and Warnana, 2018).

Synthetic studies

In order to know how robust and fast the proposed method performs, the approach is verified through application on synthetics SP data. Two synthetics data are used in this paper. The first is SP data derived from model parameters of a semi-infinite vertical cylinder. The second is SP synthetic data calculated from a sphere and a horizontal cylinder models. Both synthetic models can be seen in the Table 1 and Table 2 which both have 5% Gaussian noise added.

Single anomaly

In order to invert SP synthetic data from sphere anomaly using FPA, search space (ranges) of model parameters needed is presented as in Table 1. To invert the synthetic data and produce a robust PDM, 100 populations and 200 iterations are used. In this paper, FPA is used to determine all parameters of SP model (K, D, h, θ, and q). Figure 3a shows the synthetic data compared with the best objective function, which demonstrates that SP anomaly is close-bodied. Figure 3b shows the best, mean, and interquartile of objective function with iteration. The interquartile of objective function from all population does not always decrease with iteration increase. It means that the FPA has exploration properties. Meanwhile, the best of objective function always decreases as the iteration increases, reflecting the exploitation behaviors of FPA. Thus, FPA is able to provide balance between exploration and exploitation properties. Consequently, FPA is fit to deliver the PDM in SP anomaly inversion.

Figure 3b demonstrates that convergence between the best and mean objective function is around 0.1. Thus, the value is used as the threshold value towards delivering PDM using GLUE threshold. Figure 4 shows the histogram of PDM parameters where the highest marginal density and median of PDM (crosses) are close to the true parameters value (dots). The median and uncertainty (interquartile) value of the PDM are then presented in Table 1. It can be noted that the proposed algorithm (FPA) accurately delivers the PDM. Additionally, misfit between observed data and model responses for the best model is 1.05%. It is clearly seen that the result obtained for inverting SP data is very good.

Multiple anomalies

Table 2 shows the range of model parameters used in the inversion of SP data representing multiple anomalies. To invert the SP anomaly, 200 populations and 700 iterations are used. Figure 5a displays a comparison between synthetic and calculated SP anomalies, where the calculated SP data appears close towards the observed SP data. As described above, in order to determine the PDM, a threshold of the objective function is needed. Figure 5b demonstrates the best, mean, and interquartile of objective function for each iteration number. The mean of objective function reflects that the objective value converges around the 0.1. This value is consequently used as the threshold towards delivering PDM in this inversion. The PDM result is presented in Fig. 6. The result shows that both the highest marginal density and median of PDM (crosses) are found close towards the true model parameters (dots). Additionally, the median and uncertainty (interquartile) of PDM are demonstrated in

Table 1 Comparison of true and estimated parameters of SP anomaly disturbed with 5% Gaussian noise caused by a sphere model

Parameter	K	D	h	θ	q
True model	−100	0	15	40	0.5
Ranges of model	200 to 200	−100 to 100	0–100	0–100	0.1–1.8
Proposed algorithm	125.68 ± 40.11	1.18 ± 3.36	18.52 ± 3.70	34.01 ± 7.65	0.53 ± 0.04

Table 2 Comparison of true and estimated parameters of SP anomaly added 5% Gaussian noise caused by an inclined sheet model

Parameters	K	D	h	θ	q
True anomaly 1	1000	−100	7	40	1.5
True anomaly 2	−400	30	30	60	1
Ranges of anomaly 1	0 to 2000	−150 to −50	0–100	0–180	0.1–1.8
Ranges of anomaly 2	−700 to 700	50 to 150	0–100	0–180	0.1–1.8
Results anomaly 1	1016.62 ± 510.35	−99.61 ± 1.13	7.80 ± 1.43	36.52 ± 11.37	1.47 ± 0.10
Results anomaly 2	−405.82 ± 190.99	30.90 ± 3.44	31.92 ± 2.78	61.49 ± 6.20	1.00 ± 0.06

Table 2. The proposed algorithm has well determined the PDM in SP inversion for multiples anomalies.

Field studies

In this section, four SP anomalies with single and multiple sources are used to test the robustness of the proposed algorithm. As a general note, the steps towards determining the threshold value has not been described in further detail because it follows the same strategy as in the previous SP inversion process for synthetic anomalies.

Metallic drum anomaly

Srigutomo et al. (2006) buried a metallic drum filled with metal scrap and powder at 2.5 m in depth at N-S direction. The diameter and length of the drum were 0.6 m and 1.2 m, respectively. After a year from the buried drum, SP method was measured in W-E direction through the buried drum which the drum probably was corrosion. The center of drum is set in 0 m distance. The measured SP anomaly is shown in Fig. 7a. The SP data was analyzed by some authors using local and global optimization methods (Candra et al., 2014; Srigutomo et al., 2006; Sungkono and Warnana, 2018). Furthermore, FPA is utilized to determine SP parameters and their uncertainty parameters.

Figure 7a is comparison between observed and calculated SP data (misfit = 5.24%), while Fig. 8 shows posterior distribution model resulted by FPA method using 100 and 300 for populations and iterations, respectively. Table 3 and Fig. 7b are SP parameters in the buried metallic drum anomaly which is compared with others algorithm. The proposed algorithm is more accurate than the others. It is showed by the estimated depth using the proposed method closer with the reality of buried drum than the others. Moreover, the shape factor estimated by proposed algorithm indicates that the anomaly source is horizontal cylinder. The result is appropriate with the real source anomaly.

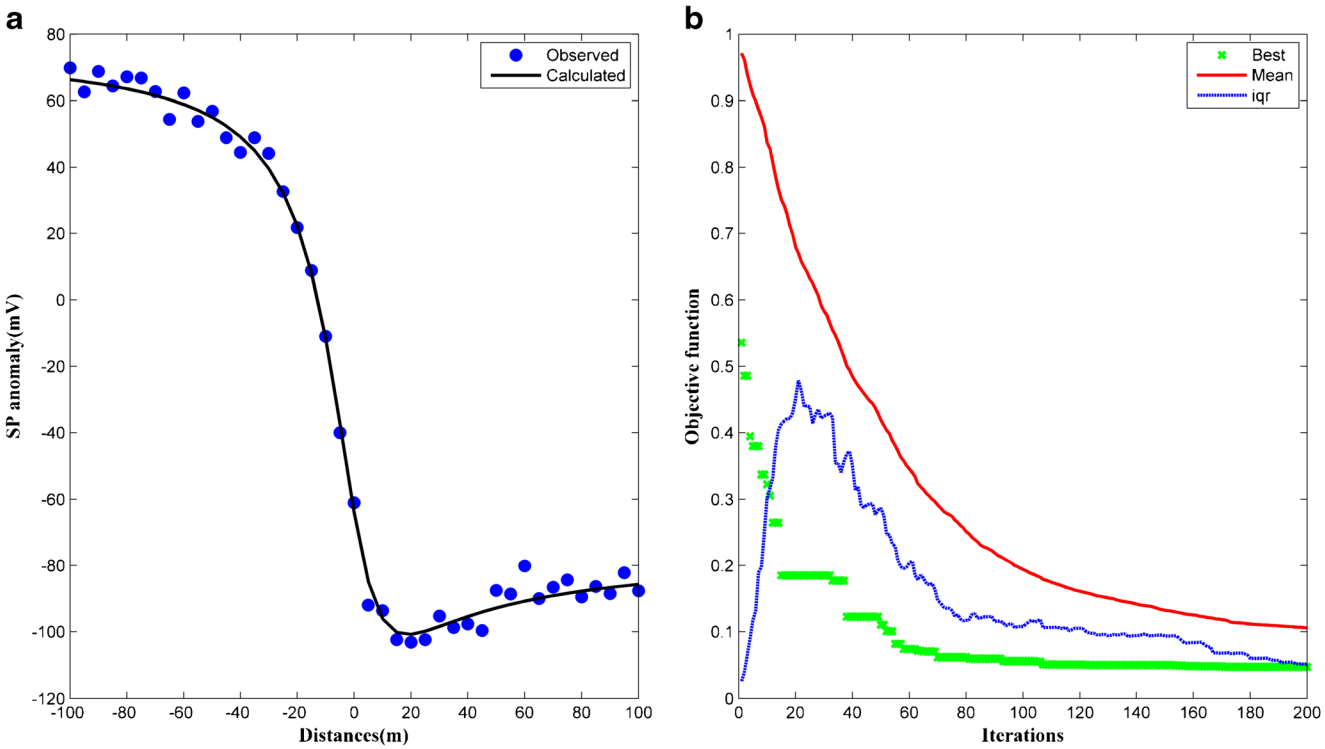

Fig. 3 (a) Noisy and inverted of synthetic SP data caused by a sphere anomaly, (b) media, interquartile, and the best of objective function for each iteration number

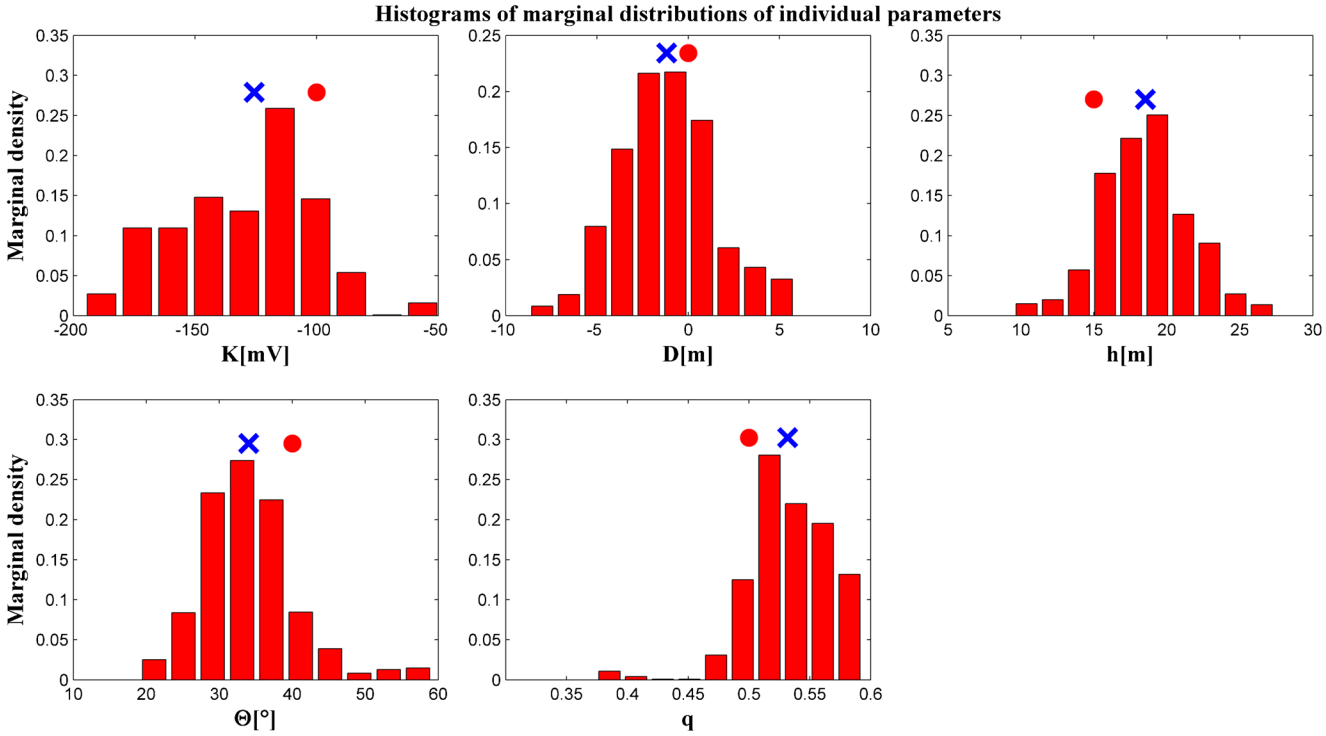

Fig. 4 Uncertainty model parameters of synthetic data

Weiss anomaly

Weiss anomaly is 1 km northwest of the Maden copper mine, where open-cut mining was being conducted. Weiss anomaly was initially measured for identifying copper mine in the Weiss, Ergani, Turkey. The SP data was broadly used to verify different algorithmic performance by various authors (Bhattacharya and Roy, 1981; El-Araby, 2004; Li and Yin,

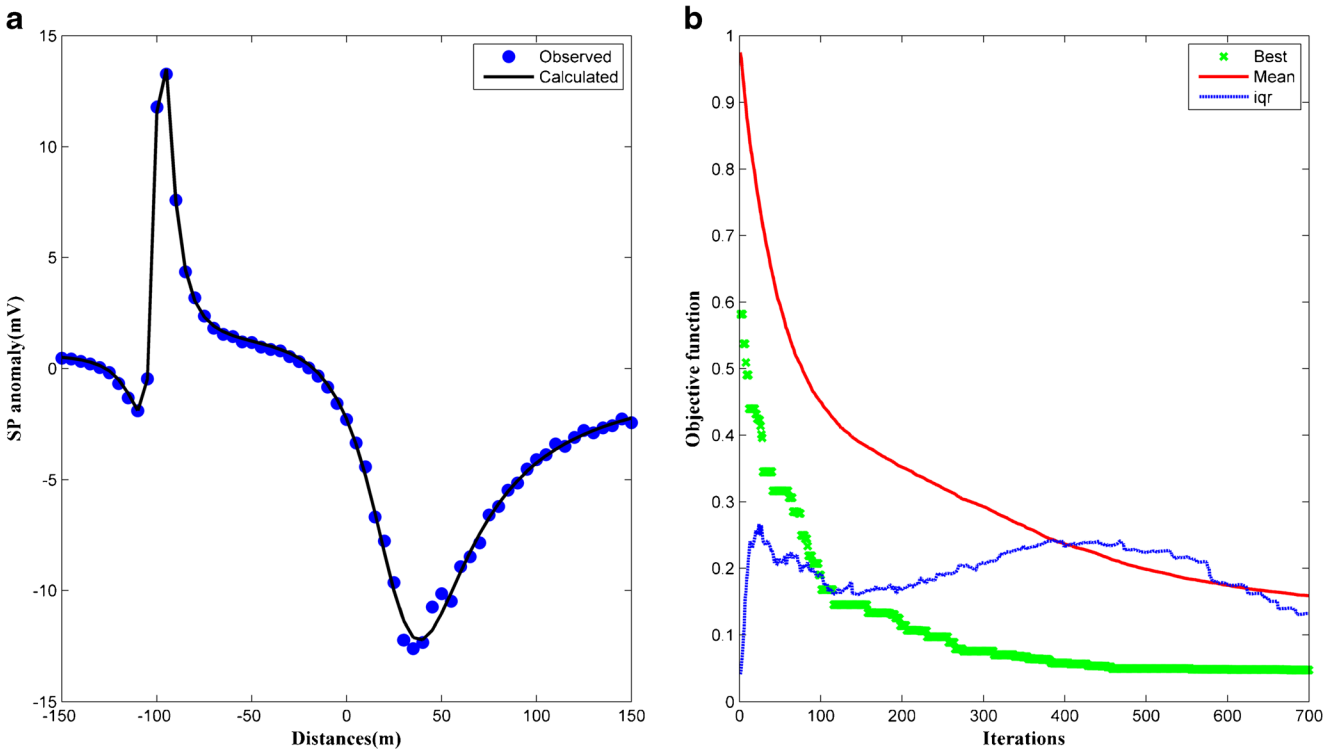

Fig. 5 (a) Noisy and inverted of synthetic SP data caused by an inclined sheet anomaly, (b) media, interquartile, and the best of objective function for each iteration number

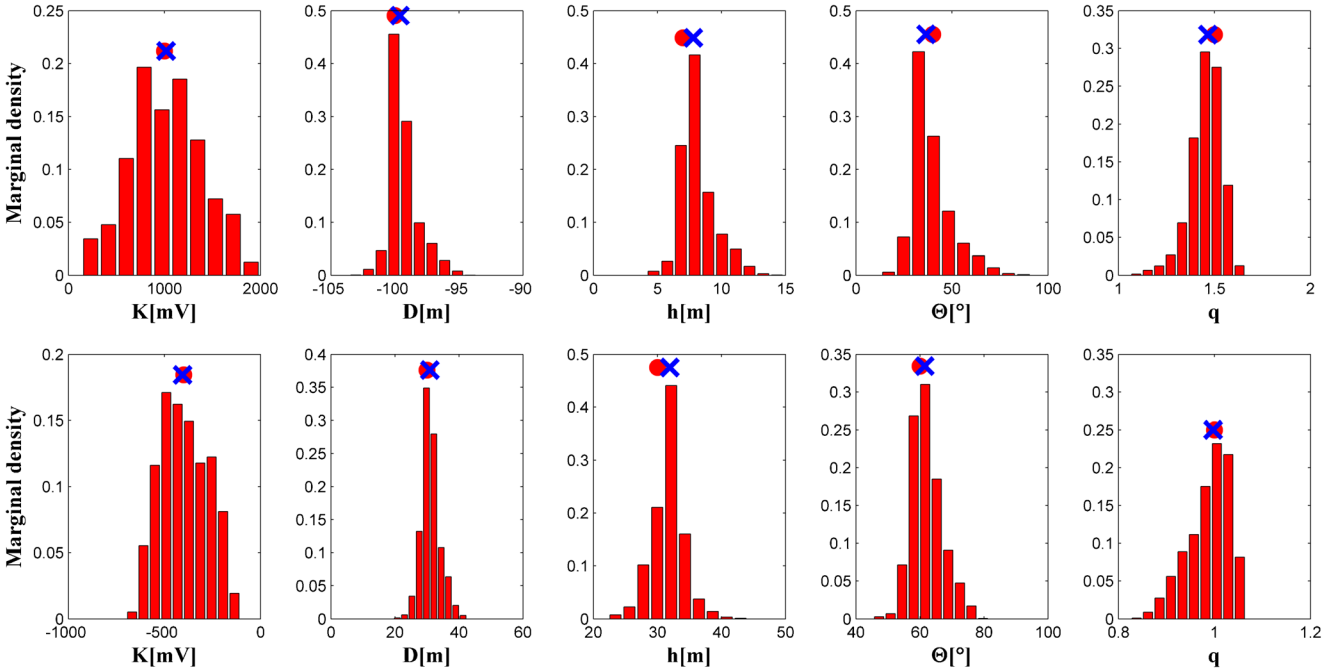

Fig. 6 Uncertainty model parameters of synthetic data

2012; Pekşen et al., 2011; Yüngül, 1950). The SP anomaly has been derived using digitalization from A to A' (dots) while the calculated SP anomaly from proposed algorithm is noted by the solid line in Fig. 9a. The misfit between predicted and observed anomaly is 10.27%.

FPA with GLUE thresholding is then applied to determine the model parameters and uncertainty of Weiss anomaly via PDM deliverance as shown in Fig. 10. The model parameters (median) and their uncertainty (interquartile) value that resulted by the proposed algorithm are given in Table 4, while Fig.

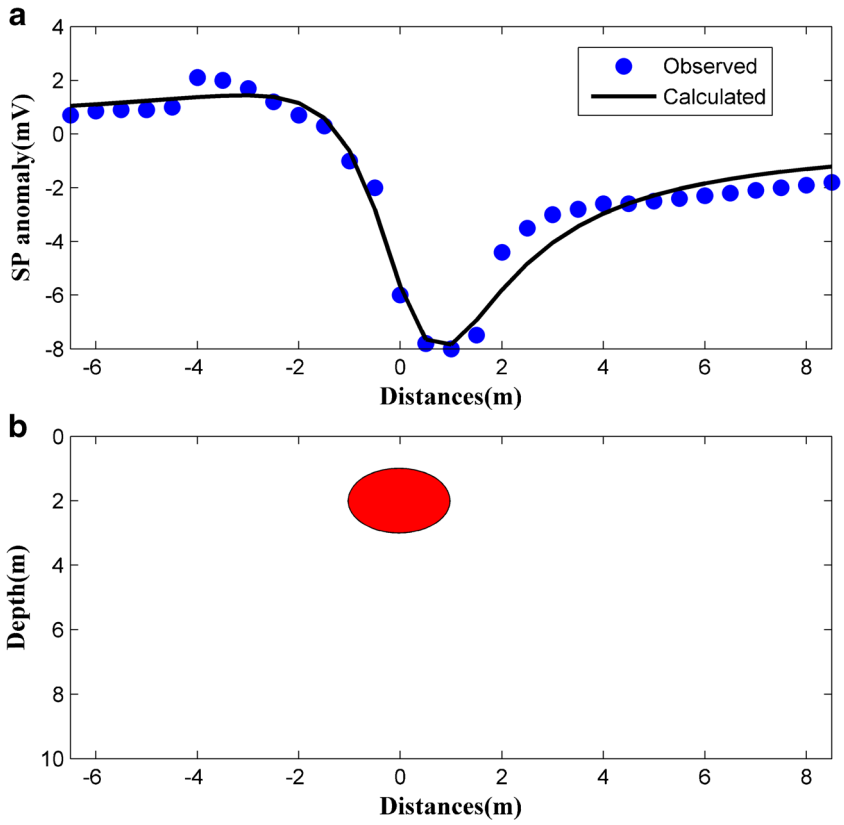

Fig. 7 Field example SP data from experimental metallic drum anomaly. (a) The observed and inverted self-potential response, (b) subsurface structure

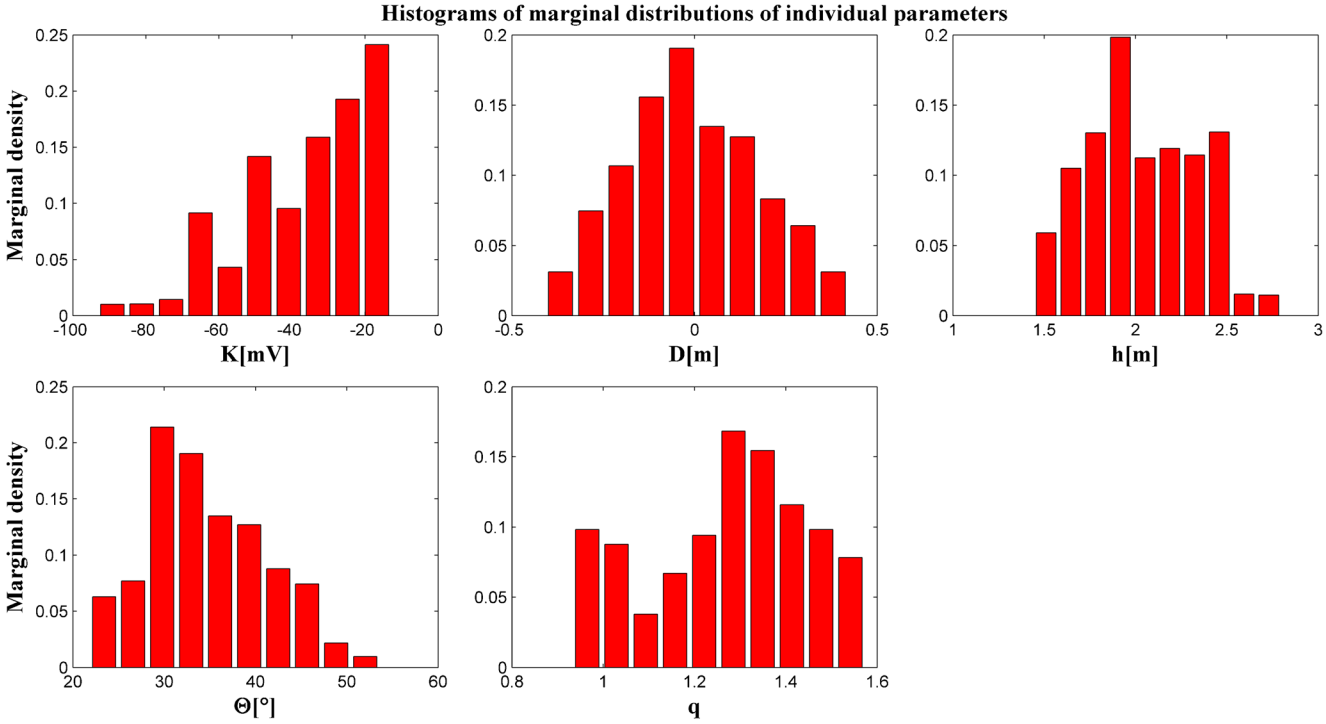

Fig. 8 Uncertainty model parameters of metallic drum anomaly

9b shows the subsurface model parameters from inverting result of Weiss anomaly. The results show that the model parameter uncertainty value is in good agreement to that of other studies. Moreover, the shape factor that resulted by the proposed method indicates that the sources of Weiss anomaly are sphere model. The result is supported by some reasons, such as: (1) the anomaly contour lines of Weiss anomaly shown are nearly circular (El-Araby, 2004); (2) the inversion process of the SP data using several idealized body approaches including sphere, horizontal cylinder, and the semi-infinite vertical cylinder shows that the best fit is the spherical model (Essa, 2011). It means that the result of the proposed algorithm is accurate to the true geological conditions.

Sawoo anomaly

The SP data measured in the Sawoo district, Ponorogo, East Java, Indonesia, was used to identify potential landslide positions. The data is measured in Mandalika formation, containing breccia, lava and tuff, sand, and silt, where there have some fissures and have landslide potential (Ramadhany et al., 2018). Field data was obtained through a fissure from the accumulation area (located in a lower position to the source area) using fix-based electrode. Closure correction is applied to remove drift effect for the field data. The SP data was then studied to verify the robustness of black hole algorithm (BHA). The parameter ranges used in the FPA correspond well with the ranges used in the BHA process, as in Table 5.

Figure 11a is a comparison between observed and calculated SP data using proposed algorithm. The calculated data appears close towards the measured data (misfit of 3.63). The PDM is then determined using GLUE threshold of objective function (threshold value: 0.18). Figure 12 shows the marginal density of model parameters (PDM) as revealed by the proposed algorithm, while Fig. 11b is subsurface model parameter from median of PDM. Finally, statistic of the PDM is presented in Table 5 together with other algorithms. The result indicates that the anomaly is a horizontal cylinder ($q \approx 1$). This correlates well to the previous BHA results which show that the landslide potential in this site is caused by a fluid channel. This channel accumulates in the bottom crack.

Table 3 Model parameter results of metallic drum anomaly inversion use proposed algorithm which is compared with other algorithms. Previous studies (Candra et al., 2014; Srigutomo et al., 2006) use assumption that *D* is zero

Parameters	K (mV)	D (m)	h (m)	θ (deg)	q
Ranges for BHA	50–50	6.5–8.5	0–50	20–100	0.3–1.8
Srigutomo et al. (2016)	−10.733	–	1.234	45.78	0.916
Candra et al. (2014)	−10.7308	–	1.2325	44.3241	0.9225
Sungkono and Warnana (2018)	9.09 ± 0.20	0.25 ± 0.04	1.15 ± 0.13	55.21 ± 1.59	0.8 ± 00
Proposed algorithm	31.47 ± 26.94	0.03 ± 0.27	1.99 ± 0.47	33.57 ± 8.83	1.29 ± 0.25

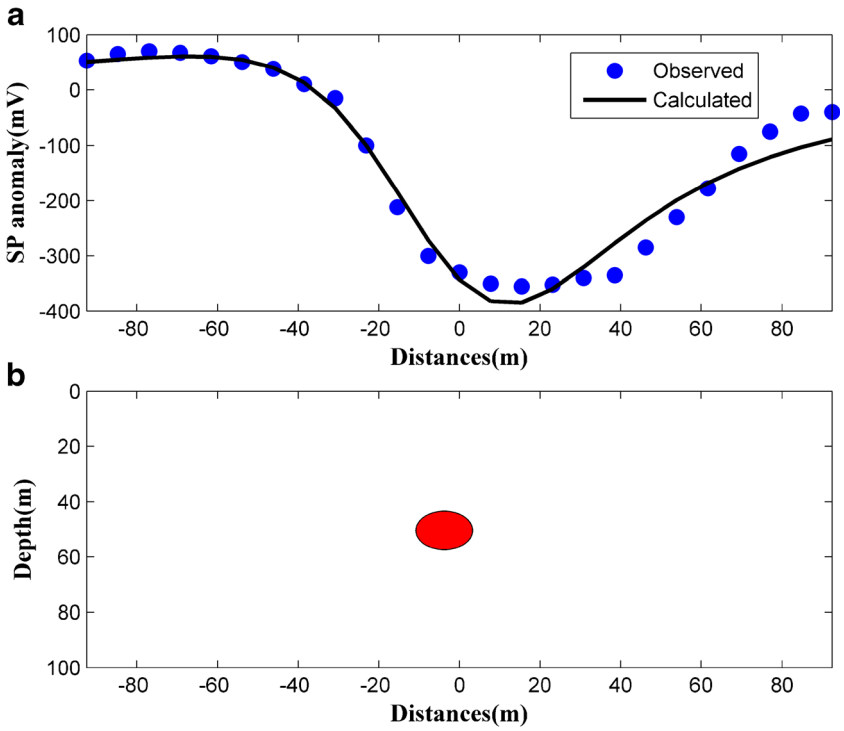

Fig. 9 Field example of the Weiss anomaly. (a) Observed and calculated SP data, (b) subsurface structure

LUSI anomaly

The LUSI embankment is an earthfill dam which was built on the alluvium. The embankment is used to resettle the results of mud erupted. High rates of mud eruption cause deformation and piping. The deformation can cause differential settlement and crack in the LUSI embankment (Sungkono et al., 2018, 2014). Rozycki et al. (2006) point out that some kinds of embankment failures can be modeled as idealized bodies. For example, piping can be represented by cylindrical bodies, internal erosion can be modeled as a sphere or point source, and differential settlement in the dam creates horizontal fractures.

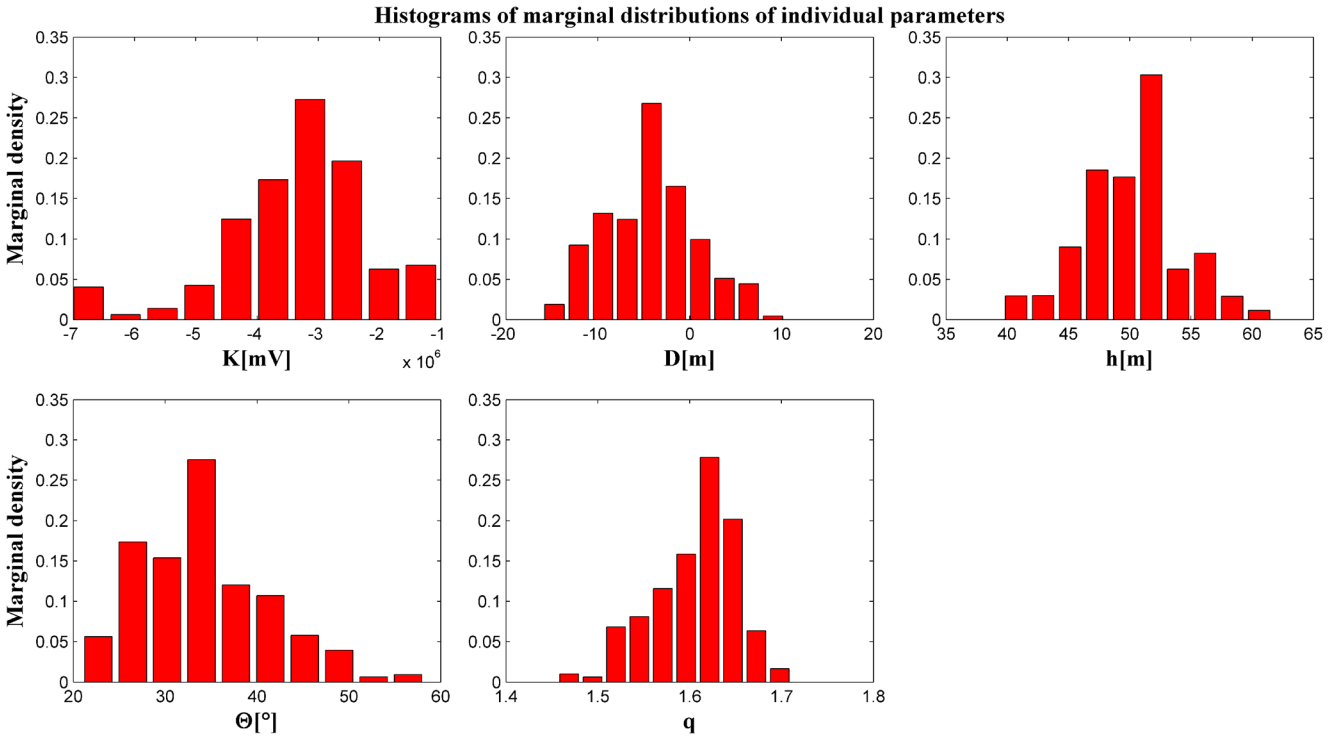

Fig. 10 Uncertainty model parameters of Weiss anomaly

Table 4 Compared result of proposed algorithm and the others for inverting SP data from Weiss anomaly

Models	K (mV)	D (m)	h (m)	θ (deg)	q
Ranges of BHA	−700,000 to 0	100 to 100	0–100	−180 to 180	0.3–1.8
Yüngül (1950)			53.8	40	1.5
Bhattacharya and Roy (1981)			54	30	1.5
El-Araby (2004)	−6256.8	0	43.37	35.89	1.464
Sungkono and Warnana (2018)	−2,698,048.70 ± 193,291.43	4.76 ± 0.50	48.06 ± 0.38	33.19 ± 0.67	1.59 ± 0.01
Proposed algorithm	−3,305,940.12 ± 1,235,956.82	3.79 ± 6.54	50.40 ± 4.67	33.46 ± 8.32	1.61 ± 0.06

The SP profile measured in the LUSI embankment at P79 to P82 was intended to identify leakage position correlating to the 2D direct resistivity and VLF-EM methods (Sungkono et al., 2018). The SP data have been used to verify robustness of black hole algorithm (BHA) (Sungkono and Warnana, 2018). The leakage position in this site is not only controlled by subsidence but also affected by fluid pressure upon the embankment. The leakage is able to flow fluids through pores and fractures (Husein et al., 2014; Sungkono et al., 2014). The LUSI area is also controlled by two faults systems, namely, Watukosek fault and Siring fault. SP anomaly acquired in this site is shown in Fig. 13a which indicates that the SP anomaly originates from more than two anomalies.

Sungkono and Warnana (2018) have analyzed the SP data using four sources anomalies. The search space of model parameters used in the FPA inversion is demonstrated in Table 6. A broad range of values has been chosen to encompass all parameters. The population and iteration numbers used in the inversion process are 200 and 1500, respectively. The inversion results using the proposed algorithm with four and five bodies are shown in Table 6 together with other different approaches. The observed SP data is compared with the calculated model response for four (dashed lines) and five (solid lines) bodies in Fig. 13a. The misfit of five anomaly bodies is 6.48, which is less than interpreting four anomaly bodies (misfit of 9.81).

Table 6 is the inverted model parameters for LUSI anomaly using FPA and BHA approaches, while Fig. 13b and c shows the subsurface structure for four and five bodies, respectively. The results show that the positions of four anomalies for both FPA interpretations are similar. Furthermore, Table 6 shows that the shape factor value for all anomalies ($q \approx 1$) can be interpreted as horizontal cylinders. Because the LUSI embankment thickness is around 15 m (Laby et al., 2016), the horizontal cylinders of the first to second anomalies (i.e., anomaly 1 and 2) may well be caused by mud flow (LUSI eruption results) movement through the LUSI embankment, known as seepage, through the embankment body as descripted in Rozycki et al. (2006). The horizontal cylinders seem to represent horizontal fractures in the embankment.

The central depths of the third and fourth anomalies appear to be deeper than the first and second anomalies. These anomalies may be in the form of horizontal fractures containing fluid as an effect of high subsidence in this site (Husein et al., 2015). Although the central depth of both anomalies is supposedly located underneath the embankment, the fracture saturation may have also hit the embankment. This prediction is supported by the presence of fluid saturation at the bottom of the embankment around where the anomaly bodies are located (Sungkono et al., 2018).

Effectiveness of FPA

Global optimization methods (GOMs) are highly potential in determining the model parameter of multiple SP anomalies, which are highly nonlinear and multimodal. Several GOMs are used to invert multiple SP anomalies, including genetic–price algorithm (GPA) (Di Maio et al., 2019), whale optimization algorithm (WOA) (Abdelazeem et al., 2019), PSO (Monteiro Santos, 2010), BHA (Sungkono and Warnana, 2018), and very fast simulated annealing (VFSA) (Sharma and Biswas, 2013). The algorithms are classified into two parts, including population-based algorithms (PBA) (GPA, WOA, PSO, BHA) and Monte Carlo based (VFSA). FPA also includes PBA.

The computational time of FPA is generally described by multiplication between population sizes and number of iterations (number of forward modeling), in which BHA has larger than the others. Moreover, using the interquartile of objective function curves, BHA shows more exploration than FPA. Consequently, FPA is more effective and efficient than BHA for providing PDM of SP data.

Table 5 Compared result of proposed algorithm and the others for SP data inversion from Sawoo anomaly

Parameters	K (mV)	D (m)	h (m)	θ (deg)	q
Ranges for BHA	1000 to 1000	0–30	0–100	0–180	0.1–1.9
Sungkono and Warnana (2018)	163.39 ± 75.80	12.01 ± 0.62	11.93 ± 0.85	82.07 ± 4.36	1.14 ± 0.10
Proposed algorithm	504.99 ± 315.01	12.94 ± 2.35	15.64 ± 3.32	91.04 ± 2.19	1.29 ± 0.12

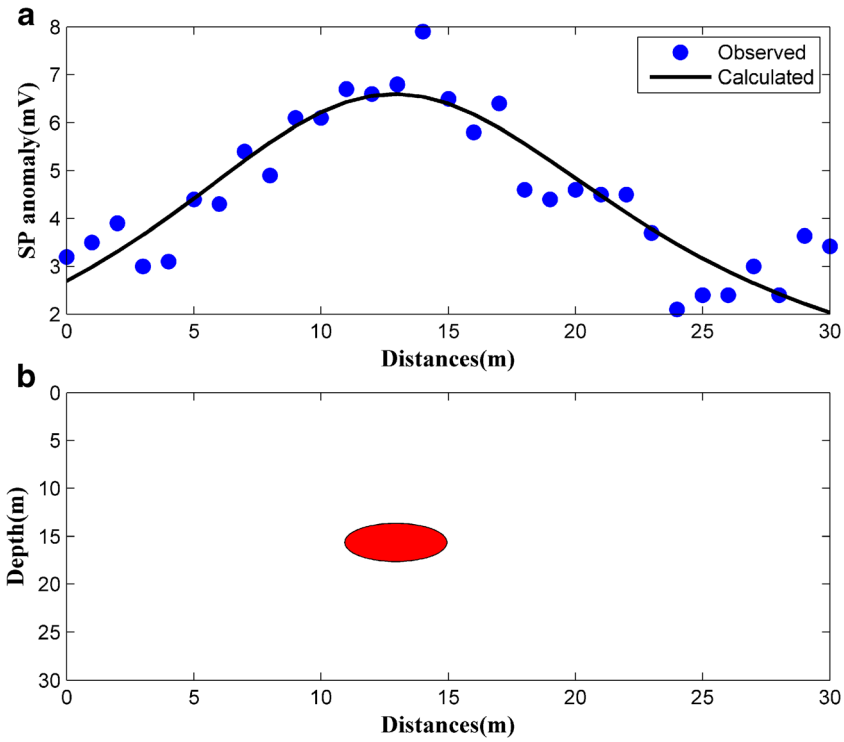

Fig. 11 Field example of Sawoo anomaly. (a) Observed and calculated SP data, (b) subsurface structure

The performance of FPA is mainly controlled by a parameter, i.e., interaction probability, which is less than the number required in PSO, GPA, and WOA that each requires three, two, and one parameters, respectively. It means that it is easier to tune parameters using FPA and WOA for inversion of SP anomalies. The efficiency of FPA compared to PSO, GPA, and WOA is equal because the computation times of the four algorithms are similar, while the affectivity of four algorithms depends on its parameter.

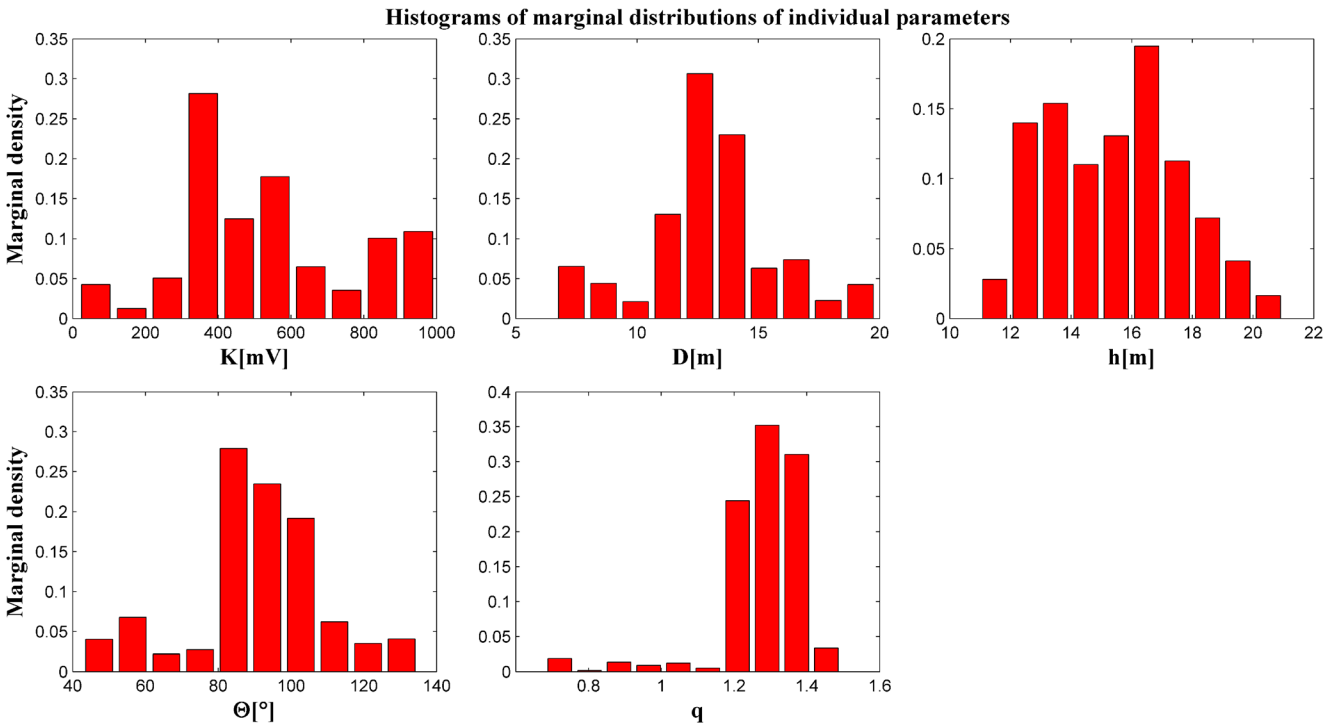

Fig. 12 Uncertainty model parameters of Sawoo anomaly

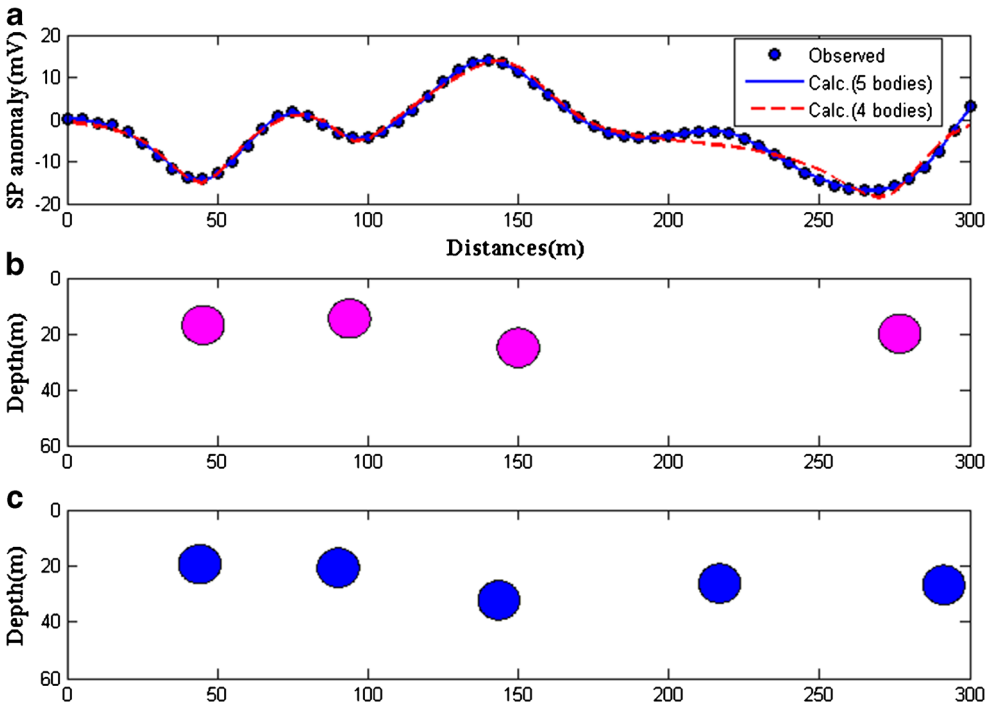

Fig. 13 Field example of the LUSI embankment anomaly. (a) Observed and calculated SP data, (b) subsurface structures for four bodies, (c) subsurface structure for five bodies

Furthermore, affectivity and efficiency of FPA are compared with VFSA. The performance of VFSA is correlated to two parameters (Sharma, 2012). Consequently, the VFSA is more complex than FPA in tuning parameters for the inversion process. However, VFSA only requires one move (one population) for each iteration. In order to find the global optimum and to provide PDM, thousands of iterations are needed in the VFSA. Consequently, VFSA is competitive with PBA.

Conclusion

Flower pollination algorithm (FPA) has been proposed to produce PDM for single and multiple SP anomalies. The approach has been verified through some synthetics and fields studies which show that the method is capable of delivering PDM of SP data with assumed models with spheres and cylinders. The results obtained from field anomalies (viz., metallic drum, Weiss, and Sawoo anomalies) showed comparable results to those by

Table 6 Compared result of proposed algorithm and others for SP data inversion from LUSI anomaly

Number of bodies		Anomalies	K	D	h	θ	q
Four bodies	Ranges parameter	Body 1	700 to 0	0–75	0–80	0–180	0.3–1.8
		Body 2	700 to 0	75–110	0–80	0–180	0.3–1.8
		Body 3	0 to 900	150–215	0–80	0–180	0.3–1.8
		Body 4	700 to 0	200–300	0–80	0–180	0.3–1.8
	Sungkono and Warnana (2018)	Body 1	412.99 ± 4.47	46.46 ± 0.60	16.16 ± 0.35	104.07 ± 1.85	1.06 ± 0.00
		Body 2	386.59 ± 11.10	99.69 ± 0.39	15.76 ± 0.59	85.88 ± 2.88	1.14 ± 0.01
		Body 3	480.60 ± 27.95	154.93 ± 0.76	25.61 ± 0.36	140.23 ± 2.02	1.01 ± 0.01
		Body 4	563.42 ± 10.49	268.04 ± 2.10	18.93 ± 0.43	103.75 ± 6.47	1.10 ± 0.00
	Present study	Body 1	470.95 ± 120.37	45.54 ± 3.65	15.23 ± 2.34	100.90 ± 15.47	1.12 ± 0.07
		Body 2	250.34 ± 122.90	101.74 ± 4.40	14.29 ± 3.76	97.73 ± 23.83	1.12 ± 0.09
		Body 3	478.29 ± 127.68	151.40 ± 1.71	22.07 ± 3.13	130.62 ± 6.53	1.03 ± 0.06
		Body 4	413.69 ± 182.87	269.49 ± 7.38	20.65 ± 2.53	107.50 ± 20.68	1.02 ± 0.07
Five bodies	Ranges parameter	Body 1	700 to 0	0–75	0–80	0–180	0.3–1.8
		Body 2	700 to 0	75–110	0–80	0–180	0.3–1.8
		Body 3	0 to 900	130–215	0–80	0–180	0.3–1.8
		Body 4	0 to 900	150–230	0–80	0–180	0.3–1.8
		Body 5	700 to 0	200–300	0–80	0–180	0.3–1.8
	Present study	Body 1	−612.44 ± 166.94	44.10 ± 1.79	19.41 ± 5.44	82.95 ± 10.57	1.06 ± 0.05
		Body 2	−411.47 ± 107.94	90.07 ± 7.67	20.66 ± 4.41	20.82 ± 39.91	1.03 ± 0.14
		Body 3	812.98 ± 121.69	143.46 ± 2.61	32.27 ± 5.94	108.00 ± 7.67	0.98 ± 0.05
		Body 4	681.77 ± 283	216.83 ± 2.52	26.25 ± 5.92	82.49 ± 11.47	1.15 ± 0.08
		5	−465.83 ± 131.50	291.32 ± 11.69	26.80 ± 5.79	170.96 ± 29.73	0.92 ± 0.04

other inversion algorithms. The SP anomaly acquired in the LUSI area shows more than three SP sources, which fits with the real conditions of four SP sources existing at different depths and locations. The results from the proposed method are also accurate to the geological information for the survey area.

Acknowledgments The research is funded by the Institute of Research and Public Services, Institut Teknologi Sepuluh Nopember, Indonesia (grant no:31467/IT2.11/PN.08/2016). Additionally, we also thank Alwi Husein and some undergraduate student in the Physics Department for helping in the field measurement.

Appendix

1: Initial parameters with switching probability $p \in [0,1]$

2: Initialize the randomly generated population within its upper and lower bounds.

3: Calculate objective function of pollen using Eq. (5)

4: Find the best solution *gbest* in the initial population

5: **while** t<tmax // tmax denotes maximum of iterations

6: **for i**=1 **to** Npollen **do** // Npollen indicates number of pollen

7: **if** rand(1)< p

8: determine global pollination move using Eq. (2)

9: **else**

10: calculate local pollen using Eq. (3)

11: **end if**

12**:** Estimate the objective function for new solution using Eq. (5).

13: Update solutions using greedy selection // Eq. (4)

14: **end for**

15: find the current best solution *gbest*

16: **end for**

References

Abdelazeem M, Gobashy M, Khalil MH, Abdrabou M (2019) A complete model parameter optimization from self-potential data using whale algorithm. J Appl Geophys 170:103825. https://doi.org/10.1016/j.jappgeo.2019.103825

Al-Saigh NH, Mohammed ZS, Dahham MS (1994) Detection of water leakage from dams by self-potential method. Eng Geol 37:115–121. https://doi.org/10.1016/0013-7952(94)90046-9

Beven K (2006) A manifesto for the equifinality thesis. J Hydrol 320:18–36. https://doi.org/10.1016/j.jhydrol.2005.07.007

Beven K, Binley A (2014) GLUE: 20 years on. Hydrol Process 28:5897–5918. https://doi.org/10.1002/hyp.10082

Beven K, Smith P (2015) Concepts of information content and likelihood in parameter calibration for hydrological simulation models. J Hydrol Eng 20:A4014010. https://doi.org/10.1061/(ASCE)HE.1943-5584.0000991

Bhattacharya B b, Roy N (1981) A note on the use of a nomogram for self-potential anomalies. Geophys Prospect 29:102–107. https://doi.org/10.1111/j.1365-2478.1981.tb01013.x

Biswas A (2017) A review on modeling, inversion and interpretation of self-potential in mineral exploration and tracing paleo-shear zones. Ore Geol Rev 91:21–56. https://doi.org/10.1016/j.oregeorev.2017.10.024

Biswas A, Sharma SP (2017) Interpretation of self-potential anomaly over 2-D inclined thick sheet structures and analysis of uncertainty using very fast simulated annealing global optimization. Acta Geod Geophys 52:439–455. https://doi.org/10.1007/s40328-016-0176-2

Biswas A, Sharma SP (2015) Interpretation of self-potential anomaly over idealized bodies and analysis of ambiguity using very fast simulated annealing global optimization technique. Surf Geophys 13:179–195. https://doi.org/10.3997/1873-0604.2015005

Biswas A, Sharma SP (2014a) Optimization of self-potential interpretation of 2-D inclined sheet-type structures based on very fast simulated annealing and analysis of ambiguity. J Appl Geophys 105:235–247. https://doi.org/10.1016/j.jappgeo.2014.03.023

Biswas A, Sharma SP (2014b) Resolution of multiple sheet-type structures in self-potential measurement. J Earth Syst Sci 123:809–825. https://doi.org/10.1007/s12040-014-0432-1

Blasone R-S, Vrugt JA, Madsen H, Rosbjerg D, Robinson BA, Zyvoloski GA (2008) Generalized likelihood uncertainty estimation (GLUE) using adaptive Markov chain Monte Carlo sampling. Adv Water Resour 31:630–648. https://doi.org/10.1016/j.advwatres.2007.12.003

Bolève A, Vandemeulebrouck J, Grangeon J (2012) Dyke leakage localization and hydraulic permeability estimation through self-potential and hydro-acoustic measurements: self-potential 'abacus' diagram for hydraulic permeability estimation and uncertainty computation. J Appl Geophys 86:17–28. https://doi.org/10.1016/j.jappgeo.2012.07.007

Candra AD, Srigutomo W, Sungkono S, B.J. (2014) A complete quantitative analysis of self-potential anomaly using singular value decomposition algorithm. In: Presented at the 2014 IEEE International Conference on Smart Instrumentation, Measurement and Applications (ICSIMA), pp 1–4. https://doi.org/10.1109/ICSIMA.2014.7047419

Cho H, Olivera F (2014) Application of multimodal optimization for uncertainty estimation of computationally expensive hydrologic models. J Water Resour Plan Manag 140:313–321. https://doi.org/10.1061/(ASCE)WR.1943-5452.0000330

Di Maio R, Piegari E, Rani P, Avella A (2016a) Self-potential data inversion through the integration of spectral analysis and tomographic approaches. Geophys J Int 206:1204–1220. https://doi.org/10.1093/gji/ggw200

Di Maio R, Piegari E, Rani P, Carbonari R, Vitagliano E, Milano L (2019) Quantitative interpretation of multiple self-potential anomaly sources by a global optimization approach. J Appl Geophys 162:152–163. https://doi.org/10.1016/j.jappgeo.2019.02.004

Di Maio R, Rani P, Piegari E, Milano L (2016b) Self-potential data inversion through a genetic-price algorithm. Comput Geosci 94:86–95. https://doi.org/10.1016/j.cageo.2016.06.005

El-Araby HM (2004) A new method for complete quantitative interpretation of self-potential anomalies. J Appl Geophys 55:211–224. https://doi.org/10.1016/j.jappgeo.2003.11.002

Essa KS (2011) A new algorithm for gravity or self-potential data interpretation. J Geophys Eng 8:434–446. https://doi.org/10.1088/1742-2132/8/3/004

Fernández-Martínez JL, Fernández-Muñiz MZ, Tompkins MJ (2012) On the topography of the cost functional in linear and nonlinear inverse problems. Geophysics 77:W1–W15. https://doi.org/10.1190/geo2011-0341.1

Husein A, Santosa BJ, Bahri AS (2015) Seepage monitoring of an embankment dam using resistivity method: a case study of LUSI mud volcano P.79 - P.82 Embankment. Appl Mech Mater 771:213–217

Husein A, Sungkono WA, Hadi S (2014) Subsurface monitoring of P.79 - P.82 LUSI embankment using GPR method to locate subsidence and possible failure, in: 15th International Conference on Ground Penetrating Radar (GPR). In: Presented at the 15th International Conference on Ground Penetrating Radar (GPR 2014), Brussels, Belgium, pp 268–273. https://doi.org/10.1109/ICGPR.2014.6970427

Jackson DD (1972) Interpretation of inaccurate, insufficient and inconsistent data. Geophys J R Astron Soc 28:97–109. https://doi.org/10.1111/j.1365-246X.1972.tb06115.x

Jagannadha Rao S, Rama Rao P, Radhakrishna Murthy IV (1993) Automatic inversion of self-potential anomalies of sheet-like bodies. Comput Geosci 19:61–73. https://doi.org/10.1016/0098-3004(93)90043-5

Laby DA, Sungkono SBJ, Bahri AS (2016) RR-PSO: fast and robust algorithm to invert Rayleigh waves dispersion. Contemp Eng Sci 9:735–741. https://doi.org/10.12988/ces.2016.6685

Lapenna V, Lorenzo P, Perrone A, Piscitelli S, Sdao F, Rizzo E (2003) High-resolution geoelectrical tomographies in the study of Giarrossa landslide (southern Italy). Bull Eng Geol Environ 62:259–268. https://doi.org/10.1007/s10064-002-0184-z

Li L, Xia J, Xu C-Y, Singh VP (2010) Evaluation of the subjective factors of the GLUE method and comparison with the formal Bayesian method in uncertainty assessment of hydrological models. J Hydrol 390:210–221. https://doi.org/10.1016/j.jhydrol.2010.06.044

Li X, Yin M (2012) Application of differential evolution algorithm on self-potential data. PLoS One 7(12):e51199. https://doi.org/10.1371/journal.pone.0051199

Łukasik S, Kowalski PA (2015) Study of flower pollination algorithm for continuous optimization, in: Intelligent Systems'2014. Springer, Cham, pp 451–459. https://doi.org/10.1007/978-3-319-11313-5_40

Maineult A, Thomas B, Nussbaum C, Wieczorek K, Gibert D, Lavielle B, Kergosien B, Nicollin F, Mahiouz K, Lesparre N (2013) Anomalies of noble gases and self-potential associated with fractures and fluid dynamics in a horizontal borehole, Mont Terri Underground Rock Laboratory. Eng Geol 156:46–57. https://doi.org/10.1016/j.enggeo.2013.01.010

Mauri G, Williams-Jones G, Saracco G (2011) MWTmat—application of multiscale wavelet tomography on potential fields. Comput Geosci 37:1825–1835. https://doi.org/10.1016/j.cageo.2011.04.005

Mauri G, Williams-Jones G, Saracco G (2010) Depth determinations of shallow hydrothermal systems by self-potential and multi-scale wavelet tomography. J Volcanol Geotherm Res 191:233–244. https://doi.org/10.1016/j.jvolgeores.2010.02.004

Mehanee SA (2014) An efficient regularized inversion approach for self-potential data interpretation of ore exploration using a mix of logarithmic and non-logarithmic model parameters. Ore Geol Rev 57:87–115. https://doi.org/10.1016/j.oregeorev.2013.09.002

Monteiro Santos FA (2010) Inversion of self-potential of idealized bodies' anomalies using particle swarm optimization. Comput Geosci 36:1185–1190. https://doi.org/10.1016/j.cageo.2010.01.011

Nasser AB, Zamli KZ, Alsewari AA, Ahmed BS (2018) Hybrid flower pollination algorithm strategies for t-way test suite generation. PLoS One 13:e0195187. https://doi.org/10.1371/journal.pone.0195187

Patella D (1997) Introduction to ground surface self-potential tomography. Geophys Prospect 45:653–681. https://doi.org/10.1046/j.1365-2478.1997.430277.x

Pekşen E, Yas T, Kayman AY, Özkan C (2011) Application of particle swarm optimization on self-potential data. J Appl Geophys 75:305–318. https://doi.org/10.1016/j.jappgeo.2011.07.013

Ramadhani I, Sungkono S (2019) A new approach to model parameter determination of self-potential data using memory-based hybrid dragonfly algorithm. Int J Adv Sci Eng Inf Technol 9:1772–1782

Ramadhany B, Sungkono RA, Warnana DD, Lestari S (2018) Comprehensive Analysis of Microtremor data to identify potential landslide (Study Case: KM23 Ponorogo-Trenggalek Road). Presented at the EAGE-HAGI 1st Asia Pacific Meeting on Near Surface Geoscience and Engineering. https://doi.org/10.3997/2214-4609.201800409

Revil A, Jardani A (2013) The self-potential method: theory and applications in environmental geosciences. Cambridge University Press, Cambridge

Rozycki A, Ruiz Fonticiella JM, Cuadra A (2006) Detection and evaluation of horizontal fractures in earth dams using the self-potential method. Eng Geol 82:145–153. https://doi.org/10.1016/j.enggeo.2005.09.013

Sadegh M, Vrugt JA, Xu C, Volpi E (2015) The stationarity paradigm revisited: hypothesis testing using diagnostics, summary metrics, and DREAM(ABC). Water Resour Res 51:9207–9231. https://doi.org/10.1002/2014WR016805

Scharnagl B, Vrugt JA, Vereecken H, Herbst M (2011) Inverse modelling of in situ soil water dynamics: investigating the effect of different prior distributions of the soil hydraulic parameters. Hydrol Earth Syst Sci 15:3043–3059. https://doi.org/10.5194/hess-15-3043-2011

Sharma SP (2012) VFSARES-a very fast simulated annealing FORTRAN program for interpretation of 1-D DC resistivity sounding data from various electrode arrays. Comput Geosci 42:177–188. https://doi.org/10.1016/j.cageo.2011.08.029

Sharma SP, Biswas A (2013) Interpretation of self-potential anomaly over a 2D inclined structure using very fast simulated-annealing global optimization — an insight about ambiguity. Geophysics 78:WB3–WB15. https://doi.org/10.1190/geo2012-0233.1

Soueid Ahmed A, Jardani A, Revil A, Dupont JP (2013) SP2DINV: A 2D forward and inverse code for streaming potential problems. Comput Geosci 59:9–16. https://doi.org/10.1016/j.cageo.2013.05.008

Srigutomo W, Agustine E, Zen MH (2006) Quantitative analysis of self-potential anomaly: derivative analysis, least-squares method and non-linear inversion. Indones J Phys 17:49–55

Sungkono, Feriadi Y, Husein A, Prasetyo H, Charis M, Irawan D, Rochman JPGN, Bahri AS, Santosa BJ (2018) Assessment of Sidoarjo mud flow embankment stability using very low frequency electromagnetic method. Environ Earth Sci 77:1–18. https://doi.org/10.1007/s12665-018-7333-6

Sungkono, Husein A, Prasetyo H, Bahri AS, Monteiro Santos FA, Santosa BJ (2014) The VLF-EM imaging of potential collapse on the LUSI embankment. J Appl Geophys 109:218–232. https://doi.org/10.1016/j.jappgeo.2014.08.004

Sungkono, Santosa BJ (2015) Differential evolution adaptive metropolis sampling method to provide model uncertainty and model selection criteria to determine optimal model for Rayleigh wave dispersion. Arab J Geosci 8:7003–7023. https://doi.org/10.1007/s12517-014-1726-y

Sungkono, Warnana DD (2018) Black hole algorithm for determining model parameter in self-potential data. J Appl Geophys 148:189–200. https://doi.org/10.1016/j.jappgeo.2017.11.015

Vrugt JA (2016) Markov chain Monte Carlo simulation using the DREAM software package: theory, concepts, and MATLAB implementation. Environ Model Softw 75:273–316. https://doi.org/10.1016/j.envsoft.2015.08.013

Vrugt JA, Beven K (2018) Embracing equifinality with efficiency: limits of acceptability sampling using the DREAM (LOA) algorithm. J Hydrol 559:954–971. https://doi.org/10.1016/j.jhydrol.2018.02.026

Yang X-S (2016) Nature-inspired optimization algorithms. Paperback reprint of hardcover, 1st ed., 2014 edn. Elsevier, Amsterdam

Yang X-S (2012) Flower pollination algorithm for global optimization, in: unconventional computation and natural computation. In: Presented at the International Conference on Unconventional Computing and Natural Computation. Springer, Berlin, pp 240–249. https://doi.org/10.1007/978-3-642-32894-7_27

Yüngül S (1950) Interpretation of spontaneous polarization anomalies caused by spheroidal ore bodies. Geophysics 15:237–246. https://doi.org/10.1190/1.1437597